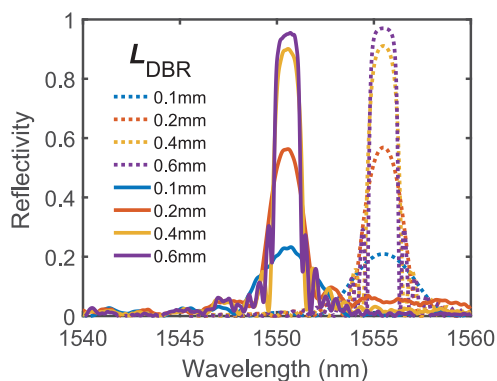


A Novel Method for Characterization of Distributed Bragg Reflectors in Photonic Integrated Circuits

Volume 10, Number 6, December 2018

Dan Zhao, *Student Member, IEEE*
Dzmitry Pustakhod, *Member, IEEE*
Kevin Williams, *Member, IEEE*
Xaveer Leijtens, *Senior Member, IEEE*






Extracted reflection spectra of DBRs at different length (solid lines) compared to the simulated ones of the reference DBRs (dashed lines).

DOI: 10.1109/JPHOT.2018.2876747

1943-0655 © 2018 CCBY

A Novel Method for Characterization of Distributed Bragg Reflectors in Photonic Integrated Circuits

Dan Zhao , *Student Member, IEEE*,
Dzmitry Pustakhod , *Member, IEEE*,
Kevin Williams, *Member, IEEE*,
and Xaveer Leijtsens , *Senior Member, IEEE*

Institute for Photonic Integration, Eindhoven University of Technology, 5612 AJ Eindhoven,
The Netherlands

DOI:10.1109/JPHOT.2018.2876747

This work is licensed under a Creative Commons Attribution 3.0 License. For more information, see
<http://creativecommons.org/licenses/by/3.0/>

Manuscript received August 31, 2018; revised October 14, 2018; accepted October 15, 2018. Date of publication October 18, 2018; date of current version November 2, 2018. This work was supported by the Memphis Project 13538, funded by the Netherlands Organization for Scientific Research (NWO) domain Applied and Engineering Sciences (TTW). Corresponding author: Dan Zhao (e-mail: d.zhao@tue.nl).

Abstract: We present a novel and accurate method for characterizing the reflection spectra of distributed Bragg reflectors using optical frequency domain reflectometry. A compact test structure with integrated reference mirror and photodetector is designed, which overcomes the dependence on the fiber-to-waveguide coupling.

Index Terms: Distributed Bragg reflectors, optical frequency domain reflectometry, photonics integration, optical spectrum.

1. Introduction

The Distributed Bragg Reflector (DBR) is an important waveguide component for achieving wavelength selective filter and reflector functions [1]. The optical reflection spectrum of a DBR records the power reflectivity of the DBR as a function of wavelength, which exposes DBR characteristics such as reflection bandwidth, Bragg wavelength, coupling coefficient and periodicity. However, accurate verification of the optical reflection spectra of DBRs on photonic integrated circuits (PICs) is a challenge due to the uncertainty induced by the fiber-to-waveguide coupling. The fiber-to-waveguide coupling leads to a coupling loss, reflections between different media and excitation of higher order modes due to alignment mismatch. The conventional methods however, are designed based on the assumption of a perfect alignment. One method is to use test structures with suppressed facet reflections, tunable laser sources (or broadband light sources) as inputs and power meters (or optical spectrum analyzers) as detectors to measure the wavelength dependence of transmitted or reflected power [2]–[4]. Not only the quality of reflection suppression affects the method accuracy but also the precision of the optical alignment. The measured spectra based on this method typically fluctuate strongly as there are interferences with reflections from the chip facets or with the excited higher order modes. Another method is to use test structures with a cleaved facet and the DBR under test to form a Fabry-Pérot cavity. The reflectivity of the DBR can be extracted from the contrast ratio between the maximum and the minimum in the fringe pattern

of intensity [5]. This method works for the extraction of the peak reflectivity but not for the full spectrum, due to the same concern for the higher order mode excitation.

A widely studied approach for characterization of fiber Bragg gratings, including their reflection spectrum, group delay and refractive index profiles, is through optical reflectometry methods [6]–[10]. The reflectometric systems such as optical time domain reflectometry (OTDR), optical coherence domain reflectometry (OCDR) and optical frequency domain reflectometry (OFDR) provide a better dynamic range of the measured reflection spectrum compared to the conventional methods [8], [9]. In addition, they allow to de-embed unwanted reflections by spatial domain filtering, which is an excellent approach to overcome the interference issues [11]. Although the reflectometry methods have been well developed for characterization of fiber Bragg gratings, it is new for Bragg gratings on PICs.

In this work, we have developed a novel and compact on-chip test structure for measuring the DBR reflection spectrum based on the OFDR method. The facet at the input side of the chip under test is as-cleaved to be used as the reference mirror in the interferometric system. This simplifies the OFDR system, as discussed in Ref. [11], [12] and removes any dependence on anti-reflection coating quality. The output of the test structure is connected to an integrated photodetector instead of a facet. The photodetector excludes reflections from the second facet and avoids one more coupling between waveguide and fiber which enables more accurate analysis [13]. In this paper, we use simulations as a first step, for the development of the numerical algorithm and for choosing the appropriate parameters for implementing the method. We present experimental demonstrations to validate the method, which show a near-perfect match with the simulations.

2. The Method

The designed structures, the data processing on the simulated results and the test structure design rules for obtaining accurate reflection spectra of DBRs are discussed in this section. Simulations are executed with our optical extensions based on modal propagation and that are implemented in Keysights Advanced Design System (ADS) [14]. The transmission and reflection properties of DBRs are calculated from scattering matrices which are determined based on calculations of the modal propagation constants and the corresponding modal field distributions.

2.1 Test Structure Simulations

A stand-alone DBR (reference) and the same DBR on a waveguide (test structure) are shown in Fig. 1(a). The stand-alone DBR is used as a reference to provide the pure transmission and reflection spectra of DBRs with certain length L_{DBR} , Bragg wavelength λ_{B} and coupling coefficient κ . The fiber-to-waveguide coupling loss and the waveguide propagation loss are set to 0. Only the TE fundamental mode is coupled into the device to avoid interference with other modes. The test structure is designed for extracting the reflection spectra of DBRs based on OFDR. It contains the same DBR as in the reference and is located on a shallow-etched waveguide at a distance L_f from the front facet. The power reflectivity of the front facet R_f is set to be the same as a cleaved facet which is 33% [15]. The reflectivity of the back facet R_b is set to be 0 to simulate full absorption by the integrated photodetector. The fiber-to-waveguide coupling efficiency is included by using the existing model in the simulation tool, which is based on modal overlap between fiber and waveguide modes. It is simulated to be 0.7 considering a perfect alignment. The waveguide propagation loss is set to be 2 dB/cm, matching previous measured values.

There are different interfering optical paths in the test structure. Path 1 is the direct signal which is used as a reference path; Path 2 represents a group of signals that have multiple distributed reflections inside the DBR; Path 3 represents a group of signals that propagate one more round-trip inside the DBR; Path 4 represents a group of signals that have a reflection from the front facet and multiple distributed reflections from the DBR; Path 5 represents a group of signals that propagate one more round-trip between the front facet and the DBR. There are more paths with multiple round-trip due to the strong reflection of DBRs, which are not shown. The transmitted power is

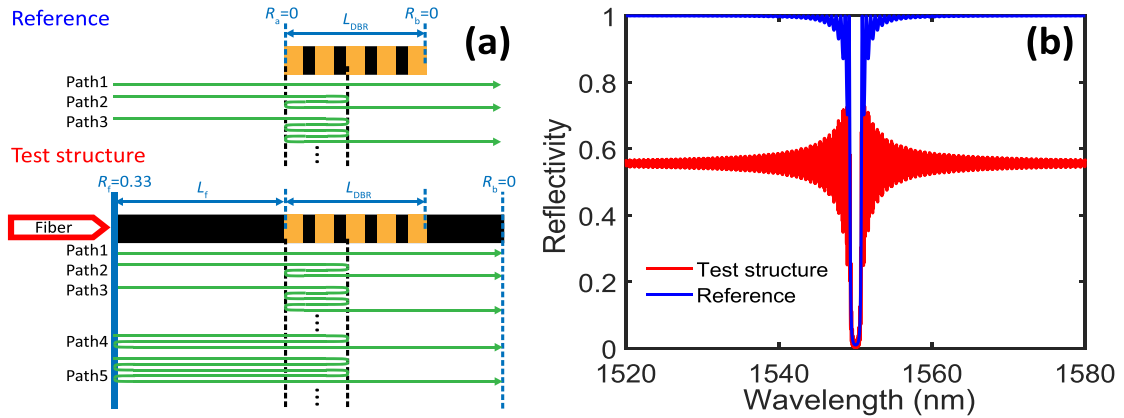


Fig. 1. (a) Structures for simulations: A stand-alone DBR with a length of L_{DBR} (reference) and the same DBR located on a shallow-etched waveguide at a distance L_f from the front facet (test structure). The R_f and R_b are the power reflectivity of the front and the back facet, respectively. In the reference DBR there are no facets, so $R_f = R_b = 0$. In the test structure the light is absorbed by the on-chip detector, so there is no back facet reflection and $R_b = 0$. The green arrows represent different paths of the transmitted signal. (b) Simulated transmission spectra of the reference (blue) and the test structure (red).

the result of the contributions of all paths. Fig. 1(b) shows the simulated transmission spectra of the reference (blue) and the test structure (red) with a DBR: $L_{\text{DBR}} = 0.6$ mm, $\lambda_B = 1550$ nm and $\kappa = 50$ cm⁻¹.

2.2 Data Processing Based on OFDR

The extraction of the DBR reflection from the modulated transmission spectrum is carried out in the following steps: first, we take the Fast Fourier transform (FFT) of the simulated spectra to retrieve a distribution map of all reflections in the spatial domain. The reflection distributions in the spatial domain for the reference (blue) and the test structure (red) are shown in Fig. 2(a). The positions of the reflection peaks are determined by the optical path length differences between different interference paths as shown in Fig. 1(a) [16]. For the reference, the two peaks at cavity length of 0 and 0.6 mm respectively represent the reflections from the entrance and the exit of the DBR due to the interference between path 1 and 2. The oscillations at higher distances are due to multiple reflections of the light within the grating structure [7]. For the test structure, there are extra reflection peaks at cavity length of 3 mm and 3.6 mm respectively due to the interference between path 1 and 4 and at cavity length of 6 mm and 6.6 mm respectively due to the interference between path 1 and 5. The oscillation period between the reflection distributions for the reference and test structure are almost identical, while an amplitude mismatch is observed.

Second, we correct the amplitude of the reflection distribution for the test structure. For the reference structure, the transmitted power at the Bragg wavelength is:

$$P_r = P_0(1 - R_{\text{DBR}}) \quad (1)$$

where P_0 is the total power input for the reference structure and equals 1; R_{DBR} is the peak reflection of the DBR at the Bragg wavelength. For the test structure, the transmitted power at the Bragg wavelength is:

$$P_t = P'_0(1 - R_{\text{DBR}})\eta \quad (2)$$

where P'_0 is the total power input for the test structure, it equals 1 in simulations but will be a different value in actual measurements; η is the power transmission coefficient determined by all the extra

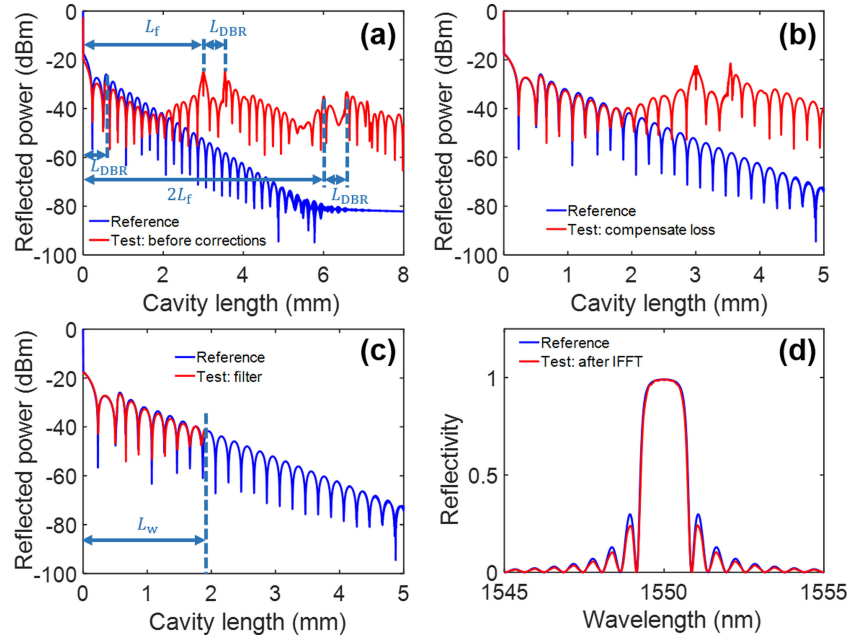


Fig. 2. Reflection distributions in the spatial domain (a) after applying a Fourier transform, (b) after compensating the losses and (c) after filtering out the unwanted reflections for the test structure (red) compared to the reflection distribution of the reference (blue); (d) The reflection spectra obtained by simulating the reference (blue) and by extracting from the test structure (red) after applying an inverse Fourier transform to the filtered reflection in the spatial domain. The L_{DBR} is the length of the DBR, the L_f is the distance between the front facet and the DBR and the L_w is the width of the filtering window.

losses in the test structure compared to the reference:

$$\eta = \eta_c(1 - R_f)\eta_t[1 + \eta_{rt} + \eta_{rt}^2 + \eta_{rt}^3 + \dots] \quad (3)$$

$$= \frac{\eta_c(1 - R_f)\eta_t}{1 - \eta_{rt}} \quad (4)$$

where the η_c , η_t and η_{rt} are the power transmission coefficients determined by the fiber-to-waveguide coupling loss, the waveguide propagation loss over the whole waveguide and over a round-trip between the front facet and the DBR, respectively. The $1 - R_f$ is the light transmittance through the front facet. The η_c is calculated from the averaged power P_a in the wavelength range outside the grating reflection band:

$$\eta_c = \frac{P_a}{P'_0(1 - R_f)\eta_t} \quad (5)$$

The power transmission determined by the round-trip loss is:

$$\eta_{rt} = R_f R_{DBR} \eta_{L_f}^2 \quad (6)$$

where η_{L_f} is the power transmission coefficient determined by the propagation loss of the waveguide over the distance L_f between the front facet and the DBR. The correction is done in linear scale with a correction ratio R_c , which can be extracted based on Eq. 1 to 6:

$$R_c = \frac{P_t}{P_r} = \frac{P_a}{P_0(1 - R_f R_{DBR} \eta_{L_f}^2)} \quad (7)$$

where the total power input P'_0 is eliminated, showing no need for the input power calibration and a simplified data analysis. The only unknown for solving the R_c is the peak reflection of the DBR

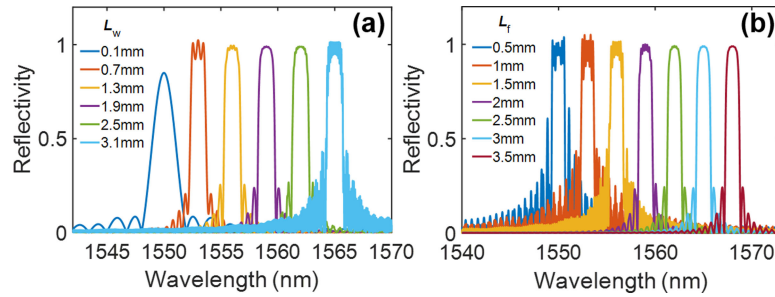


Fig. 3. The extracted reflection spectra (a) at different width of the filter window L_w and (b) while varying the distance L_f between the front facet and the DBR, respectively. The spectra are plotted with an offset of 3 nm in wavelength to make them distinguishable.

R_{DBR} . We firstly determine the R_{DBR} by choosing an R'_{DBR} arbitrarily between 0 and 1. The actual value of both will be found out later.

Third, we apply a rectangular window with a width of L_w to the spatial spectrum. This selects in the spatial domain the reflections at ΔL_{21} and ΔL_{31} and filters out the reflections at ΔL_{41} and ΔL_{51} , where ΔL_{ij} represents the path difference between path i and path j . This is possible when ΔL_{41} and ΔL_{51} are sufficiently larger than ΔL_{21} and ΔL_{31} . Defining the distance L_f between the DBR and the front facet, which determines ΔL_{41} and ΔL_{51} , and defining the filter window width L_w are discussed in the next section.

Fourth, we apply an inverse Fourier transform (IFFT) to the filtered reflection curve in spatial domain. Then the peak reflection of the DBR R_{DBR} is extracted.

The assumed peak reflection was chosen arbitrarily, and this means that the extracted peak reflection value will not match it. In order to find the correct value of the peak reflection, we sweep the assumed R'_{DBR} from 0 to 1 to retrieve the value where the extracted R_{DBR} is equal to the input value R'_{DBR} . The results with the extracted R_{DBR} for loss compensation, filtering and IFFT are shown in Fig. 2(b), (c) and (d), respectively. In Fig. 2(b), it shows that the reflection amplitudes are matched between the reference and the test structure when the cavity length is below 2 mm, the amplitudes increase at a longer cavity length due to the interference between the DBR and the front facet. In Fig. 2(c), the reflections at a longer distance than the filter window width L_w are filtered out. In Fig. 2(d), the extracted spectrum (red line) shows a perfect match of the stop-band amplitude and the position of the zero-crossings over the whole wavelength range compared to the reference. The amplitude of the side-lobe is slightly off as the loss correction ratio R_c is calculated at the Bragg wavelength.

2.3 Test Structure Design Rules

We derive the rules for defining the width of the filtering window L_w and the distance L_f between the DBR and the front facet, which are studied through simulations. Fig. 3(a) and (b) show the extracted reflection spectra at different L_w and L_f , respectively. The spectra are plotted with an offset of 3 nm in wavelength to make them distinguishable. In Fig. 3(a), the extracted spectrum shows a lower peak reflection with a small L_w of 0.1 mm. The reflection peaks are increased when the L_w is above the grating length. However, there are oscillations within the reflection band at L_w of 0.7 mm, 1.3 mm and 3.1 mm, respectively. The L_w is suggested to be longer than the triple-trip distance within the DBR: $L_w > 3L_{\text{DBR}}$ to include enough information of the DBR reflection. In addition, it should be shorter than the distance between the DBR and the front facet $L_w < L_f$ to not include the reflection peaks caused by interference between path 1 and 4. In Fig. 3(b), the oscillations disappear when the distance between the DBR and the front facet is longer than the quadruple-trip distance within the DBR: $L_f > 4L_{\text{DBR}}$.

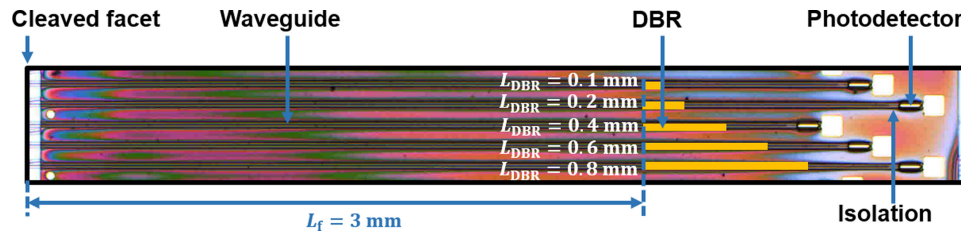


Fig. 4. Microscope photograph of a small section of the integrated chip under test. Since the buried DBRs are not visible from the original image, the orange bars are added to present the DBRs. Design values of the grating length and location are marked.

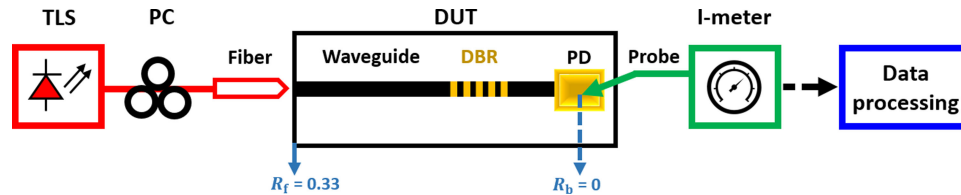


Fig. 5. A schematic diagram of the OFDR system.

3. Experimental Demonstration

3.1 Test Structures

A set of test structures with buried DBRs in shallow-etched InP waveguides [1], [17] is fabricated by Smart Photonics [18] through the JePPIX.eu multi-project wafer service [19]. Since the buried DBRs are not visible from the top image of the chip, the orange bars are added to show the lengths and the distance between the DBR and the front facet ($L_f = 3$ mm) in Fig. 4. The DBRs are designed with a Bragg wavelength of 1550 nm, a coupling coefficient of 50 cm^{-1} and length variation of 0.1, 0.2, 0.4, 0.6 and 0.8 mm, respectively. The front facet of the chip is as-cleaved, which has a power reflectivity of about 33% [15]. There are 0.1-mm-long photodetectors connected to each waveguide-end with $60\text{-}\mu\text{m}$ -long electrical isolation sections in between.

3.2 The OFDR System

A schematic diagram of the test system for the characterization of DBRs is shown in Fig. 5. Light from a tunable laser source (TLS, Agilent 81600B) is coupled into the device under test (DUT) with a lensed fiber. The input polarization direction is calibrated before the measurement. It is aligned with the chip plane which corresponds to the TE-mode of the waveguide using a polarization controller (PC). The polarization extinction ratio is 18 dB. The light intensity detected in the photodetector is resulting from the interference between all intra-chip reflections. The corresponding photocurrent is measured by a current meter (I-meter, Keithley 2602B). The data processing as discussed in Section 2-B is then performed to extract the reflection spectra of the DBRs.

3.3 Experimental Validation of the Method

Fig. 6(a) shows examples of the measured photocurrents for DBRs with the same Bragg wavelength of 1550 nm but different length of DBRs. The wavelength range is from 1520 nm to 1580 nm with a step of 10 pm. The spectra are plotted with an offset of 7 nm in wavelength to make them distinguishable in the figure. The transmission spectra are recorded by measuring the photocurrent as a function of wavelength. The photocurrent is normalized with a quadratic curve obtained by fitting the photocurrent outside of the stop-band to a second degree polynomial function. An

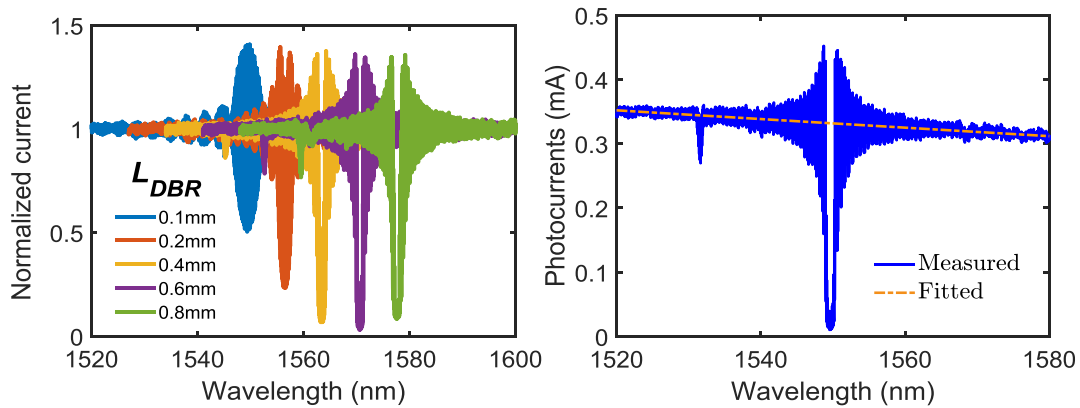


Fig. 6. (a) Measured transmission spectra of test structures with DBRs of different length. The wavelength range is from 1520 nm to 1580 nm with a step of 10 pm, the spectra are plotted with an offset of 7 nm in wavelength to make them distinguishable. (b) An example of the measured photocurrent and the fitted curve of the photocurrent outside of the stop-band to a second degree polynomial function that is used for normalization.

TABLE 1
Parameters used for Data Processing of Measured Spectra

Symbol	Parameter	Value
L_{DBR}	the length of DBRs	0.1 – 0.8 mm
L_W	the width of the filter window	$3L_f$
R_f	the power reflectivity of the front facet	33%
L_f	the distance between the front facet and the DBR	3 mm
α	the propagation loss	2 dB/cm
η_{L_f}	the power transmission coefficient considering the propagation loss over the distance L_f	0.87
P_a	the averaged photocurrent in passband	~ 0.33 mA

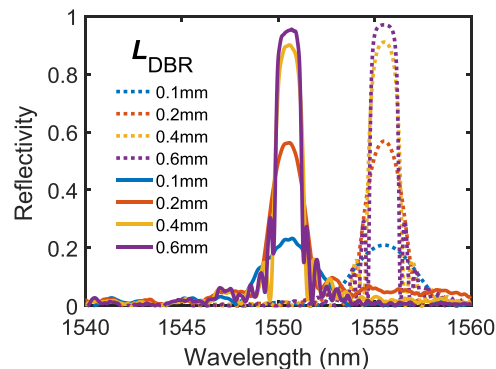


Fig. 7. Extracted reflection spectra of DBRs at different length (solid lines) compared to the simulated ones of the reference DBRs (dashed lines).

example is shown in Fig. 6(b). The transmissions of DBRs are not directly visible from the measured photocurrents due to the modulation of coupling, waveguide propagation and signal interferences.

The data processing for extracting the reflection spectra is the same as for the simulations. The used parameters are shown in Table 1. The propagation loss of the waveguides is measured by the Fabry-Pérot interferometric method [20] using other straight waveguides on the same chip. Fig. 7 shows the extracted reflection spectra (solid lines) of the same DBRs and simulated spectra (dashed lines) of the DBRs with the same lengths. The Bragg wavelength for the simulated DBRs

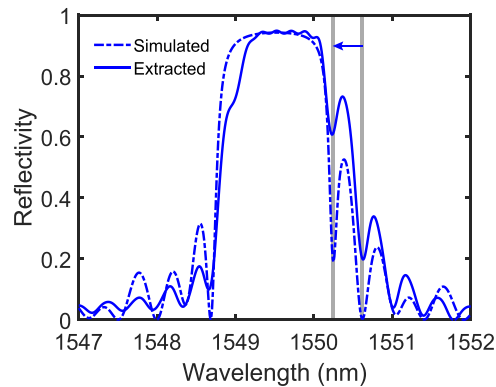


Fig. 8. Extracted reflection spectrum of a test structure with a 0.8-mm-long DBR with a stitching error at 0.5 mm from the entrance of the DBR (solid line) and simulated reflection spectrum for a reference structure with the same DBR (dashed line).

was chosen to be different to facilitate the comparison and avoid overlap with the measured spectra. There is an excellent agreement between measurement and simulation, both for the shape of the reflection spectrum and for the absolute value of the peak reflectivity.

3.4 Stitching Error Characterization

Fig. 8 shows a higher resolution response of the extracted and simulated reflection spectra of a DBR with a length of 0.8 mm. The measurement identifies a spectral asymmetry on the long wavelength side which is attributable to a stitching error induced phase shift (blue arrow) which may occur between different writing fields (each writing field is 0.5 mm) when writing DBRs with e-beam lithography [21]. In the simulation a stitching error of 20 nm, which is within the machine specification, is sufficient to match the experimental data.

4. Conclusion

We have developed a novel test structure and method based on OFDR with a subsequent filtering in the spatial domain to extract the reflectivity characteristics of DBRs. It shows an excellent agreement with simulations and it was shown to be sufficiently sensitive to analyze performance deviations due to stitching errors.

Acknowledgment

The authors acknowledge support by the Dutch Technology Foundation NWO for project 13538.

References

- [1] M. Smit *et al.*, "An introduction to InP-based generic integration technology," *Semicond. Sci. Technol.*, vol. 29, no. 8, 2014, Art. no. 083001.
- [2] A. D. Simard, Y. Painchaud, and S. LaRochelle, "Characterization of integrated Bragg grating profiles," in *Proc. Adv. Photon. Congr.*, 2012, Paper BM3D.7. [Online]. Available: <http://www.osapublishing.org/abstract.cfm?URI=BGPP-2012-BM3D.7>
- [3] C. Becker, A. Greiner, T. Oesselke, A. Pape, W. Sohler, and H. Suche, "Integrated optical Ti:Er:LiNbO₃ distributed Bragg reflector laser with a fixed photorefractive grating," *Opt. Lett.*, vol. 23, no. 15, pp. 1194–1196, Aug. 1998. [Online]. Available: <http://ol.osa.org/abstract.cfm?URI=ol-23-15-1194>
- [4] J. Pello, "Building up a membrane photonics platform in indium phosphide," Ph.D. dissertation, Dept. Elect. Eng., Eindhoven Univ. Technol., Eindhoven, The Netherlands, 2014.

- [5] B. Docter, F. Karouta, E. Bente, T. de Smet, and M. Smit, "Short-cavity lasers with deeply etched DBR mirrors for photonic integrated circuits," in *Proc. 13th Annu. Symp. IEEE/LEOS Benelux Chapter*, Enschede, The Netherlands, Nov. 2008, pp. 39–42.
- [6] A. Ozcan, M. J. F. Digonnet, and G. S. Kino, "Characterization of fiber Bragg gratings using spectral interferometry based on minimum-phase functions," *J. Lightw. Technol.*, vol. 24, no. 4, pp. 1739–1757, Apr. 2006.
- [7] P. Lambelet, P. Y. Fonjallaz, H. G. Limberger, R. P. Salathe, C. Zimmer, and H. H. Gilgen, "Bragg grating characterization by optical low-coherence reflectometry," *IEEE Photon. Technol. Lett.*, vol. 5, no. 5, pp. 565–567, May 1993.
- [8] S. D. Dyer, K. B. Rochford, and A. H. Rose, "Fast and accurate low-coherence interferometric measurements of fiber Bragg grating dispersion and reflectance," *Opt. Exp.*, vol. 5, no. 11, pp. 262–266, Nov. 1999. [Online]. Available: <http://www.opticsexpress.org/abstract.cfm?URI=oe-5-11-262>
- [9] S. Keren, A. Rosenthal, and M. Horowitz, "Measuring the structure of highly reflecting fiber Bragg gratings," *IEEE Photon. Technol. Lett.*, vol. 15, no. 4, pp. 575–577, Apr. 2003.
- [10] S. Keren and M. Horowitz, "Interrogation of fiber gratings by use of low-coherence spectral interferometry of noiselike pulses," *Opt. Lett.*, vol. 26, no. 6, pp. 328–330, Mar. 2001. [Online]. Available: <http://ol.osa.org/abstract.cfm?URI=ol-26-6-328>
- [11] D. Zhao, D. Pustakhod, K. Williams, and X. Leijtens, "High resolution optical frequency domain reflectometry for analyzing intra-chip reflections," *IEEE Photon. Technol. Lett.*, vol. 29, no. 16, pp. 1379–1382, Aug. 2017.
- [12] D. Melati, A. Alippi, and A. Melloni, "Waveguide-based technique for wafer-level measurement of phase and group effective refractive indices," *J. Lightw. Technol.*, vol. 34, no. 4, pp. 1293–1299, Feb. 2016.
- [13] D. Zhao, D. Pustakhod, L. Augustin, J. Bolk, K. Williams, and X. Leijtens, "Optical frequency domain reflectometry for characterization of distributed Bragg reflectors," in *Proc. 19th Eur. Conf. Int. Opt.*, Eindhoven, The Netherlands, Apr. 2017.
- [14] X. Leijtens, P. Le Lourec, and M. Smit, "S-matrix oriented CAD-tool for simulating complex integrated optical circuits," *J. Sel. Topics Quantum Electron.*, vol. 2, no. 2, pp. 257–262, Jun. 1996.
- [15] P. Besse, J. Gu, and H. Melchior, "Reflectivity minimization of semiconductor laser amplifiers with coated and angled facets considering two-dimensional beam profiles," *IEEE J. Quantum Electron.*, vol. 27, no. 6, pp. 1830–1836, Jun. 1991.
- [16] U. Glombitza and E. Brinkmeyer, "Coherent frequency-domain reflectometry for characterization of single-mode integrated-optical waveguides," *J. Lightw. Technol.*, vol. 11, no. 8, pp. 1377–1384, Aug. 1993.
- [17] D. Zhao, L. M. Augustin, J. Bolk, D. Pustakhod, K. A. Williams, and X. J. M. Leijtens, "Distributed Bragg reflectors on InP platform fabricated with deep-UV technology," in *Proc. 21st Annu. Symp. IEEE Photon. Soc. Benelux Chapter*. Ghent, Belgium, Nov. 2016, pp. 231–234.
- [18] [Online]. Available: <http://www.smartphotonics.nl/>
- [19] X. Leijtens, "JePPIX: The platform for InP-based photonics," *IET Optoelectronics*, vol. 5, no. 5, pp. 202–206, 2011.
- [20] T. Feuchter and C. Thirstrup, "High precision planar waveguide propagation loss measurement technique using a Fabry-Pérot cavity," *IEEE Photon. Technol. Lett.*, vol. 6, no. 10, pp. 1244–1247, Oct. 1994.
- [21] D. Zhao, L. M. Augustin, D. Pustakhod, K. A. Williams, and X. J. M. Leijtens, "Design of uniform and non-uniform DBR gratings using transfer-matrix method," in *Proc. IEEE Photon. Soc. Symp. (Benelux Chapter)*, P. Kockaert, P. Emplit, S.-P. Gorza, and S. Massar, Eds., Brussels, Belgium, Nov. 2015, pp. 87–90.